

Improving Signed Propagation for Graph Neural Networks

Yoonhyuk Choi¹, Jiho Choi¹, Taewook Ko¹ and Chong-Kwon Kim²

¹Seoul National University

²Korea Institute of Energy Technology

{younhyuk95, jihochoi, taewook.ko}@snu.ac.kr, ckim@kentech.ac.kr

Abstract

Message-passing Graph Neural Networks (GNNs), which collect information from adjacent nodes achieve dismal performance on heterophilic graphs. Various schemes have been proposed to solve this problem, and propagating signed information on heterophilic edges has gained great attention. Recently, some works provided theoretical analysis that signed propagation always leads to performance improvement under a binary class scenario. However, we notice that prior analyses do not align well with multi-class benchmark datasets. This paper provides a new understanding of signed propagation for multi-class scenarios and points out two drawbacks in terms of message-passing and parameter update: (1) Message-passing: if two nodes belong to different classes but have a high similarity, signed propagation can decrease the separability. (2) Parameter update: the prediction uncertainty (e.g., conflict evidence) of signed neighbors increases during training, which can impede the stability of the algorithm. Based on the observation, we introduce two novel strategies for improving signed propagation under multi-class graphs. The proposed scheme combines calibration to secure robustness while reducing uncertainty. We show the efficacy of our theorem through extensive experiments on six benchmark graph datasets.

1 Introduction

The increase in graph-structured datasets has led to rapid advancements in graph mining techniques including random walk-based node embedding and graph neural networks (GNNs). Especially, GNNs provide satisfactory performances in various applications including node classification and link prediction. The main component of GNNs is message-passing [Gilmer *et al.*, 2017], where the information is propagated between nodes and then aggregated. Also, the integration of a structural property with the node features enhances the representation and the discrimination powers of GNNs substantially [Defferrard *et al.*, 2016; Kipf and Welling, 2016; Velickovic *et al.*, 2017].

Early GNN schemes assume the network homophily where nodes of similar attributes make connections with each other based on the social influence theory [McPherson *et al.*, 2001]. Especially, spectral GNNs [Defferrard *et al.*, 2016; Kipf and Welling, 2016; Wang and Zhang, 2022] perform Laplacian smoothing (a.k.a low-pass filtering) to receive low-frequency signals from neighbor nodes. Consequently, these methods fail to adequately deal with heterophilous graphs [Zhu *et al.*, 2020; Luan *et al.*, 2022] such that even a simple MLP outperforms GNN in some cases. To relieve this problem, a plethora of clever algorithms (spatial GNNs) have been proposed including the adjustment of edge coefficients [Velickovic *et al.*, 2017; Brody *et al.*, 2021], aggregation of remote nodes with high similarity [Pei *et al.*, 2020; Liu *et al.*, 2021; Li *et al.*, 2022]. However, the majority of prior schemes [Ma *et al.*, 2021] stipulate certain conditions of advantageous heterophily and these constraints undermine their applicability in real-world benchmark datasets.

Recently, some bodies of work allow the edge coefficients to be negative [Chien *et al.*, 2020; Bo *et al.*, 2021] to preserve high-frequency signal exchanges between neighbors. Further, from the perspective of gradient flow, [Di Giovanni *et al.*, 2022] shows that negative eigenvalue preserves the high-frequency signals to dominate during propagation. Instead of changing the signs of edges, [Luo *et al.*, 2021] assigns zero-weights (block information) to disassortative connections precluding message diffusion on such edges. Here, there arises a question: *does signed messaging always yield better results than blocking information on heterophilic edges?*

To answer the above question, we conduct an empirical study and illustrate its results in Figure 2. Along with this, we aim to establish theoretical properties to compare their discrimination power. For this, recent studies [Ma *et al.*, 2021; Yan *et al.*, 2021] scrutinize the changes in node features before and after message reception. Here, they provide some useful insights into using signed messages based on the node’s relative degree and its homophily ratio. Nonetheless, prior analyses were confined to binary class graphs, which may detriment their applicability to generic graphs. In this paper, we extend the theorem to a multi-class scenario positing that the blind application of signed messages to multi-class graphs may increase the uncertainty of predictions. Throughout this analysis, we suggest employing confidence calibration [Guo *et al.*, 2017; Wang *et al.*, 2021] which is simple yet

effective to enhance the quality of predictions. To summarize, our contributions can be described as follows:

- Contrary to prior work confined to a binary class, we tackle the signed messaging mechanism in a multi-class scenario. Our work provides fundamental insight into using signed messages and establishing the theoretical background for the development of powerful GNNs.
- We conjecture and prove that signed propagation reduces the discrimination power during inference for some cases, and also increases the uncertainty in predictions. Based on this understanding, we propose novel strategies using two types of calibration.
- We conduct extensive experiments on six benchmark datasets to validate our theorems and show the effectiveness of calibration.

2 Related Work

Graph Neural Networks (GNNs). Under semi-supervised settings, GNNs have shown great potential by utilizing the information of adjacent nodes. Early GNN studies [Bruna *et al.*, 2013; Defferrard *et al.*, 2016] focused on the spectral graph analysis (e.g., Laplacian decomposition) in a Fourier domain. However, they suffer from large computational costs as the scale of the graph increases. GCN [Kipf and Welling, 2016] reduced the overhead by harnessing the localized spectral convolution through the first-order approximation of a Chebyshev polynomial. Another notable approach is spatial-based GNNs [Velickovic *et al.*, 2017; Brody *et al.*, 2021] which aggregate information in a Euclidean domain. Early spatial techniques became a stepping stone to many useful schemes that encompass relevant remote nodes as neighbors.

GNNs on heterophilous graphs. Traditional message-passing GNNs fail to perform well in heterophilic graphs [Pei *et al.*, 2020]. To redeem this problem, recent studies have paid attention to the processing of disassortative edges [Derr *et al.*, 2018; Huang *et al.*, 2019] by capturing the difference between nodes or incorporating distant but similar nodes as neighbors. Similarly, H₂GCN [Zhu *et al.*, 2020] separates ego and neighbors during aggregation. LS-GNN [Chen *et al.*, 2023] suggests a long-range aggregation scheme and EvenNet [Lei *et al.*, 2022] receives messages from even-hop away nodes only. As another branch, [Li *et al.*, 2022] selects neighbors from the nodes without direct connections. Configuring path-level pattern [Sun *et al.*, 2022], finding a compatibility matrix [Zhu *et al.*, 2021], and employing adaptive propagation [Wang *et al.*, 2022] have also been proposed recently. Another school of methodologies either changes the sign of disassortative edges from positive to negative [Chien *et al.*, 2020; Bo *et al.*, 2021; Fang *et al.*, 2022; Guo and Wei, 2022] or assigns zero-weights to disassortative edges [Luo *et al.*, 2021]. Even though these schemes show their effectiveness [Baranwal *et al.*, 2021] on binary classes, it may require further investigations before extending their applications to a multi-class scenario.

3 Preliminary

Let $\mathcal{G} = (\mathcal{V}, \mathcal{E}, X)$ be a graph with $|\mathcal{V}| = n$ nodes and $|\mathcal{E}| = m$ edges. The node attribute matrix is $X \in \mathbb{R}^{n \times F}$, where F is the dimension of an input vector. Given X , the hidden representation of node features $H^{(l)}$ (l -th layer) is derived through message passing. Here, node i 's feature is the row of $h_i^{(l)}$. The structural property of \mathcal{G} can be represented by its adjacency matrix $A \in \{0, 1\}^{n \times n}$. Also, D is a diagonal matrix with node degrees $d_{ii} = \sum_{j=1}^n A_{ij}$. Each node has its label $Y \in \mathbb{R}^{n \times C}$, where C represents the number of classes. The global edge homophily ratio (\mathcal{H}_g) is defined as:

$$\mathcal{H}_g \equiv \frac{\sum_{(i,j) \in \mathcal{E}} \mathbb{1}(Y_i = Y_j)}{|\mathcal{E}|}. \quad (1)$$

Likewise, the local homophily (b_i) of node i is given as:

$$b_i \equiv \frac{\sum_{j=1}^n A_{ij} \cdot \mathbb{1}(Y_i = Y_j)}{d_{ii}}. \quad (2)$$

The goal of semi-supervised node classification is to predict the class of unlabeled nodes $\mathcal{V}_U = \{\mathcal{V} - \mathcal{V}_L\} \subset \mathcal{V}$ given the partially labeled training set \mathcal{V}_L .

4 Theoretical Analysis

We first discuss the mechanism of Message-Passing Neural Networks (MPNN) and the definition of using signed messages (§ 4.1). Then, we introduce the previous analysis of employing signed propagation on binary class graphs (§ 4.2) and point out some misunderstandings through the empirical analysis on real-world graphs (§ 4.3). Through this, we extend them to a multi-class scenario and define the drawbacks of signed propagation under this condition (§ 4.4).

4.1 Message-Passing Neural Networks

Generally, Graph Neural Networks (GNNs) employ the strategy of propagation and then aggregation, where the node features are updated iteratively. This is widely known as message-passing, which can be represented as follows:

$$H^{(l+1)} = \phi(\bar{H}^{(l+1)}), \quad \bar{H}^{(l+1)} = AH^{(l)}W^{(l)}. \quad (3)$$

$H^{(0)} = X$ is the initial vector and $H^{(l)}$ is nodes' hidden representations at the l -th layer. $\bar{H}^{(l+1)}$ is retrieved through message-passing (A) and we obtain $H^{(l+1)}$ after an activation function ϕ (e.g. ReLU). $W^{(l)}$ is the trainable weight matrices that are shared across all nodes. The final prediction is produced by applying cross-entropy $\sigma(\cdot)$ (e.g., log-softmax) to $\bar{H}^{(L)}$ and the loss function is defined as:

$$\mathcal{L}_{GNN} = \mathcal{L}_{nll}(Y, \hat{Y}), \quad \hat{Y} = \sigma(\bar{H}^{(L)}). \quad (4)$$

The parameters are updated by computing negative log-likelihood loss \mathcal{L}_{nll} between the predictions (\hat{Y}) and true labels (Y). Generally, most GNNs assume homophily and tend to preserve the low-frequency information (local smoothing) [Nt and Maehara, 2019]. Consequently, they fail to capture the difference between node features and achieve lower performance on the heterophilous networks [Oono and Suzuki, 2019; Pei *et al.*, 2020].

4.2 Using signed messages on binary classes

Recent studies [Chien *et al.*, 2020; Bo *et al.*, 2021; Yan *et al.*, 2021; Chen *et al.*, 2022] emphasize the importance of high-frequency signals and suggest flipping the sign of disassortative edges from positive to negative. To analyze the usefulness of signed messages, we provide a theoretical analysis of using signed messages under a *binary class* from message-passing (Eq. 3) and parameter update (Eq. 4) perspective.

(Binary class, message-passing) Signed propagation always improves the discrimination power. To prove this, we analyze the movements of node features [Baranwal *et al.*, 2021] using three types of propagation (original, signed, and zero-weights). For brevity, we employ GCN [Kipf and Welling, 2016] as a base model. Firstly, let us assume a binary classification task ($y_i \in \{0, 1\}$) and inherit several useful notations [Yan *et al.*, 2021] for simplifications: **(1)** For all nodes $i = \{1, \dots, n\}$, their degrees $\{d_i\}$ and features $\{h_i\}$ are i.i.d. random variables. **(2)** Every class has the same population. **(3)** With a slight abuse of notation, assume that $h^{(0)} = XW^{(0)}$ is the first layer projection of initial node features. **(4)** The node feature of label y_i follows the distribution (μ or $-\mu$) below:

$$\mathbb{E}(h_i^{(0)}|y_i) = \begin{cases} \mu, & \text{if } y_i = 0 \\ -\mu, & \text{if } y_i = 1. \end{cases} \quad (5)$$

Prior work [Yan *et al.*, 2021] introduces Theorems 4.1, 4.2 using the local homophily (Eq. 2), message passing (Eq. 3), and expectation of node features (Eq. 5). Each theorem below utilizes the original and signed propagation, respectively.

Theorem 4.1 (Binary class, vanilla GCN). *Let us assume $y_i = 0$. Then, the expectation after a single-hop propagation $\mathbb{E}(h_i^{(1)})$ is defined as:*

$$\mathbb{E}(h_i^{(1)}|y_i, d_i) = \frac{(2b_i - 1)d'_i + 1}{d_i + 1} \mathbb{E}(h_i^{(0)}|y_i), \quad (6)$$

where $d'_i = \sum_{j \in \mathcal{N}_i} \sqrt{\frac{d_i + 1}{d_j + 1}}$.

Proof is provided in App. A.1.

The generalized version of the above theorem is described in [Ma *et al.*, 2021], which takes two distributions μ_0, μ_1 as:

$$h_i \sim N(b_i\mu_0 + (1 - b_i)\mu_1, \frac{1}{\sqrt{d_i + 1}}). \quad (7)$$

Eq. 7 reduces to Eq. 6 when $\mu_1 = -\mu_0$.

Theorem 4.2 (Binary class, signed GCN). *If the sign of heterophilous edges is flipped correctly under the error ratio (e), the expectation is given by:*

$$\mathbb{E}(h_i^{(1)}|y_i, d_i) = \frac{(1 - 2e)d'_i + 1}{(d_i + 1)} \mathbb{E}(h_i^{(0)}|y_i). \quad (8)$$

Proof can be seen in App. A.2.

Referring to the above analyses, we can induce the expectation of zero-weight GCN as below:

Theorem 4.3 (Binary class, zero-weight GCN). *Similar to the Theorem 4.2, assigning zero weights to the heterophilous edges leads to the following feature distribution:*

$$\mathbb{E}(h_i^{(1)}|y_i, d_i) = \frac{(b_i - e)d'_i + 1}{(d_i + 1)} \mathbb{E}(h_i^{(0)}|y_i). \quad (9)$$

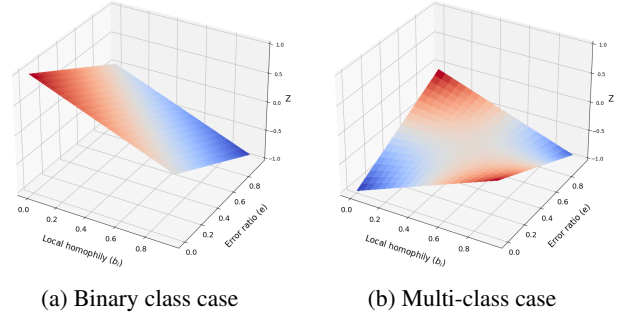


Figure 1: We plot the Z (Eq. 10 and 18) to compare the discrimination power of signed and zero-weight GCNs. The red and blue colored parts indicate the regions where signed GCN and zero-weight GCN have better performance, respectively

Proof can be found in App. A.3.

For all theorems, if the coefficient of $\mathbb{E}(h_i^{(0)}|y_i)$ is smaller than 1, the node feature moves towards the decision boundary and message passing loses its discrimination power [Yan *et al.*, 2021]. Based on this observation, we can compare the discrimination powers of signed and zero-weight GCNs.

Corollary 4.4 (Binary class, the difference of discrimination power between signed and zero-weight GCN). *Omitting the overlapping part of Theorems 4.2 and 4.3, their difference, Z , can be induced by the error ratio (e) and homophily (b_i):*

$$Z = (1 - 2e) - (b_i - e) = 1 - e - b_i, \quad (10)$$

where $0 \leq e, b_i \leq 1$.

Here, we visualize the above value Z in Fig. 1a. Note that the space is half-divided by the plane $Z = 0$ since $\int_0^1 \int_0^1 (1 - e - b_i) de db_i = 0$. When e and b_i are small, Z tends to be positive, indicating that signed GCN outperforms zero-weight GCN and vice versa.

(Binary class, parameter update) Signed propagation well separates the ego and neighbors. Let us assume an ego node i and its neighbor node j are connected with a signed edge. Please ignore other neighbor nodes to concentrate on the mechanism of signed messaging. Firstly, we can obtain the output of node i as:

$$\hat{Y}_i = \sigma(\bar{H}_i^L) = \sigma\left(\frac{\bar{H}_i^{(L)}}{d_i + 1} - \frac{\bar{H}_j^{(L)}}{\sqrt{(d_i + 1)(d_j + 1)}}\right). \quad (11)$$

Assuming that the label of the ego (Y_i) is k , the loss (\mathcal{L}_{nll}) between a true label $Y_i \in \mathcal{R}^C$ and a prediction $\hat{Y}_i \in \mathcal{R}^C$ can be defined as below:

$$\mathcal{L}_{nll}(Y_i, \hat{Y}_i) = -\log(\hat{y}_{i,k}) \quad (12)$$

Since the column-wise components of the last weight matrix $W^{(L)}$ act as an independent classifier, we can infer that the probability of node j being a class k ($\hat{y}_{j,k}$) transitions in the opposite to the node i 's probability ($\hat{y}_{i,k}$) as the training epoch (t) proceeds:

$$\hat{y}_{j,k}^{(t+1)} < \hat{y}_{j,k}^t, \quad \hat{y}_{i,k}^{(t+1)} > \hat{y}_{i,k}^t \quad (13)$$



Figure 2: Node classification accuracy on six benchmark datasets. Firstly, vanilla GCN utilizes the original graph. The coefficient of heterophilous edges is changed to -1 in signed GCN and to 0 in zero-weight GCN, respectively. Signed GCN (+ calib) employs two types of calibration, which are introduced in Section 5

since $\hat{y}_{i,k}^{(t+1)} = \hat{y}_{i,k}^t - \eta \nabla_i \mathcal{L}_{nll}(Y_i, \hat{Y}_i)$ and $\hat{y}_{j,k}^{(t+1)} = \hat{y}_{j,k}^t - \eta \nabla_j \mathcal{L}_{nll}(Y_i, \hat{Y}_i)$. Notation η is the learning ratio and a symbol ∇ represents a partial derivative of the loss function.

Proof of Eq. 13 is in App. A.4.

4.3 Empirical Analysis

To verify whether Corollary 4.4 is applicable to real-world data, we conduct an empirical analysis. Here, we measure the node classification accuracy of GCN [Kipf and Welling, 2016] using six benchmark graphs (the statistical details are shown in Table 2). From the original graph (vanilla GCN), we fabricate two graph variants; one that replaces disassortative edges with -1 (signed GCN), and the other that assigns zero-weights on heterophilous connections (zero-weight GCN). Since we identified all heterophilous edges, the error ratio is zero ($e = 0$). Thus, regarding Corollary 4.4, signed GCN should outperform zero-weight GCN, where $Z (= 1 - b_i)$ has a non-negative value regardless of the homophily ratio ($0 \leq b_i \leq 1$). However, Fig. 2 shows that zero-weight GCN generally outperforms signed GCN ($Z \leq 0$). Thus, we extend the above theorems to cover a multi-class scenario and introduce two types of calibration in §5, where the signed GCN (+ calib) achieves the best performance using these strategies.

4.4 Using signed messages on multiple classes

To renovate the previous understandings, we extend the environment to multiple classes and point out some drawbacks of using signed propagation from two perspectives.

(Multi-class, message-passing) Signed propagation decreases the discrimination power under certain conditions. Without loss of generality, one needs to extend the assumptions in Eq. 5 to multiple classes. For this, we employ spherical coordinates assuming 3 class datasets as below:

$$\mathbb{E}(h_i^{(0)}|y_i) = (\mu, \phi, \theta), \quad (14)$$

where μ also represents the scale of a vector. The direction of the vector is determined by the angles ϕ and θ . The above equation also satisfies the origin symmetry under the binary class ($C = 2$) since $(\mu, \pi/2, 0) = -(\mu, \pi/2, \pi)$. Through this, we can redefine Thm. 4.1 and 4.2 for multi-class GCNs as follows.

Theorem 4.5 (Multi-class, signed GCN). *Let us assume the label $y_i = 0$. For simplicity, we denote the coordinates of the ego $(\mu, \pi/2, 0)$ as k , and its neighbors (μ, ϕ', θ') as k' . Then, the expectation of $h_i^{(1)}$ is defined to be:*

$$\mathbb{E}(h_i^{(1)}|y_i, d_i) = \frac{(1 - 2e)\{b_i k + (b_i - 1)k'\}d'_i + k}{d_i + 1}. \quad (15)$$

Proof is provided in App. B.1.

Theorem 4.6 (Multi-class, zero-weight GCN). *Likewise, the $h_i^{(1)}$ driven by zero-weight GCN is:*

$$\mathbb{E}(h_i^{(1)}|y_i, d_i) = \frac{\{(1 - e)b_i k + e(1 - b_i)k'\}d'_i + k}{d_i + 1}. \quad (16)$$

Proof is provided in App. B.2.

Similar to Corollary 4.4, we can compare the separability of the two methods based on their coefficients.

Corollary 4.7 (Multi-class). *The difference of discrimination power (Z) between signed and zero-weight GCN in the multi-class case is:*

$$Z = -eb_i k + (1 - e)(b_i - 1)k' \quad (17)$$

Then, we can induce the conditional statement as below based on the distribution of aggregated neighbors (k'):

$$Z \in \begin{cases} 1 - e - b_i, & \text{if } k' = -k \\ -2eb_i - (1 - e - b_i), & \text{if } k' = k. \end{cases} \quad (18)$$

More details can be found in App. B.3.

Fig. 1b plots Z for the multi-class case. The above corollary implies that if the distribution of aggregated neighbor is origin symmetry ($k' = -k$), $Z (= 1 - e - b_i)$ becomes identical to the Eq. 10. Under this condition, signed propagation might perform well. However, as k' gets closer to k , its discrimination power degrades (Z gets smaller) as shown in the blue areas in Fig. 1b, where $\int_0^1 \int_0^1 (-2eb_i + e + b_i - 1) dedb_i = -1$. Intuitively, the probability of being $k' = -k$ may decrease as the number of classes increases, which means that the zero-weight GCN generally outperforms the signed GCN in multi-class graphs. This result is consistent with our empirical analysis in Fig. 2, where signed GCN slightly outperforms zero-weight GCN only on Pubmed, which has the smallest number of classes among six datasets (Table 2).

(Multi-class, parameter update) Signed propagation contributes to the ego-neighbor separation, but it also increases the uncertainty of the predictions. Adequate uncertainty management is vital in machine learning to generate highly confident predictions [DeVries and Taylor, 2018; Moon *et al.*, 2020; Mukherjee and Awadallah, 2020]. This is closely related to the entropy (e.g., information gain [Liu *et al.*, 2022]) and recent work [Kendall and Gal, 2017] formulates two types of uncertainties: the *aleatoric* and *epistemic* caused by the data and the model, respectively. But here, we rather focus on the conflict evidence (*dissonance*) [Perry, 2013; Zhao *et al.*, 2020], which ramps up the entropy of outputs. One can easily measure the uncertainty of a prediction (\hat{y}_i) using Shannon's entropy [Shannon, 1948] as:

$$E(\hat{y}_i) = - \sum_{j=1}^C \hat{y}_{i,j} \log_c \hat{y}_{i,j}. \quad (19)$$

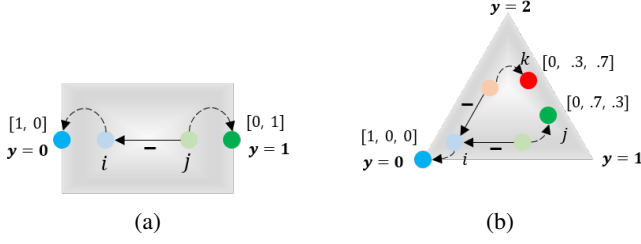


Figure 3: Assume Dirichlet distribution: (a) In binary class, signed propagation contributes to the separation of neighbor node (j) and reduces the entropy. (b) In multiple classes, the uncertainty of neighboring nodes that are connected with signed edges (j, k) increases

Using the above equation, we can induce the last theorem as below.

Theorem 4.8. *Under multiple classes, the signed messages also contribute to ego-neighbor separation. However, the entropy of signed neighbors $E(\hat{y}_s)$ gets greater than the plane (or zero) ones $E(\hat{y}_p)$ in proportion to the training epoch (t) as below:*

$$\begin{aligned} \hat{y}_{j,k}^{(t+1)} &< \hat{y}_{j,k}^t, \quad \hat{y}_{i,k}^{(t+1)} > \hat{y}_{i,k}^t, \\ E(\hat{y}_s^{(t+1)}) - E(\hat{y}_p^{(t+1)}) &> E(\hat{y}_s^t) - E(\hat{y}_p^t). \end{aligned} \quad (20)$$

Proof with an example can be seen in the App. C.

For a better understanding, we visualize the influence of signed propagation through Dirichlet distribution in Figure 3. Under binary class (Fig 3a), signed propagation separates the two nodes and reduces uncertainty. Similarly, we can also see that the class probability ($y = 0$) of signed neighbors j, k decreases under multiple classes (Fig 3b). Nevertheless, the simultaneous increase in class probability ($y = 1, 2$) in nodes i, j leads to the increment of uncertainty (Thm. 4.8), which may harm the stability of GNNs.

5 Methodology

In Section 4.4, we pointed out the drawbacks of using signed propagation from two perspectives: message-passing and parameter update. Based on this observation, we propose two types of calibration to relieve such limitations. Calibration is one type of self-training method [Guo *et al.*, 2017; Yang *et al.*, 2021] that acts as a regularization term. Even though it has shown to be effective for generic GNNs [Wang *et al.*, 2021], we notice that the performance gain is much greater when integrated with signed methods.

5.1 (Message-Passing) Edge weight calibration

In Corollary 4.7, we analyze the impact of signed propagation based on the distribution of neighbors k' . It was observed that as k' is similar to k , signed propagation reduces the discrimination power. Thus, we propose the following strategies: (1) During the validation/test phase, we block the information propagation of highly similar nodes, which may decrease the discrimination power. (2) Instead, for training, we do not employ edge weight calibration to enhance the separability of two nodes. Our method can act as a downstream task of GNNs, where the score (e.g., cosine similarity) of two

nodes can be simply calculated based on their l -th layer node features as follows:

$$\cos(h_i^l, h_j^l) = \frac{h_i^l \cdot h_j^l}{\|h_i^l\|_2 \|h_j^l\|_2}. \quad (21)$$

During inference, we replace the signed edges a_{ij} (e.g., attention values) as 0, which satisfies the following condition:

$$\forall (i, j) \in \mathcal{E}, \quad a_{ij} = \begin{cases} 0 & \text{if } a_{ij} < 0 \wedge \cos(h_i^l, h_j^l) > \epsilon \\ a_{ij} & \text{otherwise} \end{cases}. \quad (22)$$

Here, ϵ is a hyper-parameter (threshold). Through this, we can ensure separability during training and maintain a discrimination power during the inference phase.

5.2 (Parameter update) Confidence calibration

In Theorem 4.8, we show that signed messages increase the uncertainty of predictions. Thus, we propose a simple yet effective solution to reduce uncertainty by calibrating the predictions. The proposed method is free from entire path configuration, cost-efficient, and fairly powerful. The loss function for confidence calibration can be defined as below:

$$\mathcal{L}_{conf} = \frac{1}{n} \sum_{i=1}^n (-\max(\hat{y}_i) + \text{submax}(\hat{y}_i)), \quad (23)$$

where $n = |\mathcal{V}_{valid} \cup \mathcal{V}_{test}|$ is the set of validation and test nodes. Our method is quite similar to prior work [Wang *et al.*, 2021], but we do not utilize the label of validation sets for a fair comparison. As defined above, it penalizes the maximal and sub-maximal values to be similar in order to suppress the generation of conflict evidence, which can reduce the side-effect in Theorem 4.8.

Remark. The proposed strategies are highly scalable for signed GNNs [Chien *et al.*, 2020; Bo *et al.*, 2021; Yan *et al.*, 2021]. The edge weight calibration (Eq. 22) only requires a similarity score between two nodes, and the confidence calibration (Eq. 23) just utilizes the predictions (\hat{y}).

5.3 Optimization

To reduce the uncertainty of signed GNNs, we take confidence calibration (Eq. 23) for optimization as below:

$$\mathcal{L}_{total} = \mathcal{L}_{GNN} + \lambda \mathcal{L}_{conf}. \quad (24)$$

Here, \mathcal{L}_{GNN} indicates the cross-entropy loss of any GNNs (Eq. 4), and λ is a hyper-parameter that balances the influence of calibration. After finishing training, edge weight calibration (Eq. 22) is applied during the inference phase. Using these strategies, in Figure 2, we can see that the signed GCN (+ calib) achieves a significant improvement compared to the signed GCN, which justifies our analysis.

We introduce the pseudo-code of calibrated FAGCN [Bo *et al.*, 2021] and time complexity in App. D.

6 EXPERIMENTS

We conducted extensive experiments to validate our theorems and to compare the performances of our method and baselines. We aim to answer the following research questions:

Table 1: (Q1) Node classification accuracy (%) with standard deviation on six datasets. **Bold** and underline indicates the 1st and 2nd best performance. Values in bracket stand for the dissonance defined in Eq. 25 and symbol ‡ means that calibration is applied to baseline method

Datasets \mathcal{H}_g (Eq. 1)	Cora 0.81	Citeseer 0.74	Pubmed 0.8	Actor 0.22	Chameleon 0.23	Squirrel 0.22
GCN	79.0 ± 0.6 (0.17)	67.5 ± 0.8 (0.29)	77.6 ± 0.2 (0.53)	20.2 ± 0.4 (0.29)	49.3 ± 0.5 (0.19)	31.7 ± 0.7 (0.31)
GCN ‡	81.0 ± 0.9 (0.12)	71.3 ± 1.2 (0.14)	77.8 ± 0.4 (0.38)	21.7 ± 0.6 (0.62)	49.4 ± 0.6 (0.25)	31.5 ± 0.6 (0.58)
GAT	80.1 ± 0.6 (0.22)	68.0 ± 0.7 (0.25)	78.0 ± 0.4 (0.45)	22.5 ± 0.3 (0.28)	47.9 ± 0.8 (0.17)	30.8 ± 0.9 (0.27)
GAT ‡	81.4 ± 0.4 (0.12)	72.2 ± 0.6 (0.08)	78.3 ± 0.3 (0.39)	23.2 ± 1.8 (0.43)	49.2 ± 0.4 (0.16)	30.3 ± 0.8 (0.40)
APPNP	81.3 ± 0.5 (0.15)	68.9 ± 0.3 (0.21)	79.0 ± 0.3 (0.42)	23.8 ± 0.3 (0.49)	48.0 ± 0.7 (0.34)	30.4 ± 0.6 (0.69)
GCNII	81.1 ± 0.7 (0.08)	68.5 ± 1.4 (0.13)	78.5 ± 0.4 (0.20)	25.9 ± 1.2 (0.43)	48.1 ± 0.7 (0.21)	29.1 ± 0.9 (0.24)
H ₂ GCN	80.6 ± 0.6 (0.16)	68.2 ± 0.7 (0.22)	78.5 ± 0.3 (0.29)	25.6 ± 1.0 (0.34)	47.3 ± 0.8 (0.19)	31.3 ± 0.7 (0.62)
PTDNet	81.2 ± 0.9 (0.24)	69.5 ± 1.2 (0.42)	78.8 ± 0.5 (0.44)	21.5 ± 0.6 (0.33)	50.6 ± 0.9 (0.17)	<u>32.1</u> ± 0.7 (0.34)
PTDNet ‡	81.9 ± 0.6 (0.20)	71.1 ± 0.8 (0.31)	79.0 ± 0.2 (0.38)	22.7 ± 0.6 (0.19)	50.9 ± 0.3 (0.15)	32.3 ± 0.5 (0.30)
GPRGNN	82.2 ± 0.4 (0.25)	70.4 ± 0.8 (0.43)	79.1 ± 0.1 (0.26)	25.4 ± 0.5 (0.55)	49.1 ± 0.7 (0.25)	30.5 ± 0.6 (0.36)
GPRGNN ‡	84.5 ± 0.2 (0.04)	<u>73.2</u> ± 0.5 (0.05)	80.0 ± 0.2 (0.11)	27.7 ± 1.3 (0.33)	<u>50.7</u> ± 0.4 (0.18)	31.6 ± 0.4 (0.16)
FAGCN	80.9 ± 0.5 (0.15)	69.8 ± 0.6 (0.17)	79.0 ± 0.5 (0.31)	25.2 ± 0.8 (0.66)	46.5 ± 1.1 (0.25)	30.4 ± 0.4 (0.64)
FAGCN ‡	<u>83.7</u> ± 0.4 (0.09)	73.7 ± 0.5 (0.08)	<u>79.7</u> ± 0.2 (0.16)	<u>27.3</u> ± 0.5 (0.42)	48.6 ± 0.7 (0.13)	31.3 ± 0.5 (0.37)
GGCN	80.0 ± 1.2 (0.38)	69.7 ± 1.6 (0.30)	78.2 ± 0.4 (0.47)	22.5 ± 0.5 (0.47)	48.5 ± 0.7 (0.15)	30.2 ± 0.7 (0.40)
GGCN ‡	83.4 ± 0.8 (0.07)	73.1 ± 0.4 (0.05)	78.7 ± 0.3 (0.29)	24.1 ± 0.4 (0.26)	49.8 ± 0.4 (0.07)	30.8 ± 0.6 (0.15)

Table 2: Statistical details of six benchmark datasets

Datasets	Cora	Citeseer	Pubmed	Actor	Cham.	Squirrel
# Nodes	2,708	3,327	19,717	7,600	2,277	5,201
# Edges	10,558	9,104	88,648	25,944	33,824	211,872
# Features	1,433	3,703	500	931	2,325	2,089
# Labels	7	6	3	5	5	5

- **Q1** Is the calibration improves the node classification accuracy of graph neural networks?
- **Q2** Do the signed messages increase the uncertainty of the final prediction?
- **Q3** How much impact do the two calibration methodologies have on performance improvement?
- **Q4** How does the hyper-parameter ϵ (Eq. 22) and λ (Eq. 24) affect on the overall performance?

Datasets. The statistical details of datasets are in Table 2. (1) *Cora*, *Citeseer*, *Pubmed* [Kipf and Welling, 2016] are citation graphs, where a node corresponds to a paper and edges are citations between them. The labels are the research topic of the papers. (2) *Actor* [Tang *et al.*, 2009] is a co-occurrence graph where actors and co-occurrences in the same movie are represented as nodes and edges, respectively. The labels are five types of actors. (3) *Chameleon*, *Squirrel* [Rozemberczki *et al.*, 2019] are Wikipedia hyperlink networks. Each node is a web page and the edges are hyperlinks. Nodes are categorized into five classes based on monthly traffic.

Baselines. We employ several state-of-the-art methods for validation: (1) GNNs with positive edge weights: GCN [Kipf and Welling, 2016], GAT [Velickovic *et al.*, 2017], APPNP [Klicpera *et al.*, 2018], GCNII [Chen *et al.*, 2020], and H₂GCN [Zhu *et al.*, 2020]. (2) Edge pruning GNN: PTDNet [Luo *et al.*, 2021]. (3) GNNs with signed propagation: GPRGNN [Chien *et al.*, 2020], FAGCN [Bo *et al.*, 2021], and GGCN [Yan *et al.*, 2021].

Details of baseline and their implementation are in App. E.

6.1 (Q1) Experimental results

In Table 1, we describe the node classification accuracy of each method. Further, we show the dissonance (*diss*) of each method in a bracket, which measures uncertainty and is powerful in distinguishing out-of-distribution data from conflict predictions [Zhao *et al.*, 2020; Huang *et al.*, 2022]:

$$diss(\hat{y}_i) = \sum_{j=1}^C \left(\frac{\hat{y}_{ij} \sum_{k \neq j} \hat{y}_{ik} (1 - \frac{|\hat{y}_{ik} - \hat{y}_{ij}|}{\hat{y}_{ij} + \hat{y}_{ik}})}{\sum_{k \neq j} \hat{y}_{ik}} \right). \quad (25)$$

The above value is defined only for \hat{y}_i with non-zero elements. Now, let us analyze the results from two perspectives.

Homophily ratio plays an important role in GNNs. Three citation networks have higher homophily compared to others. We can see that all methods perform well under homophilic datasets. As homophily decreases, methods that adjust weights depending on associativity outperform plain GNNs. Similarly, using signed messages (GPRGNN, FAGCN, and GGCN) or the separation of ego and neighbors (H₂GCN) has shown to be effective here. For some graphs where many nodes share the same neighborhoods (Chameleon, Squirrel) [Platonov *et al.*, 2023], we notice that blocking information (PTDNet) achieves better performance than signed GNNs.

Calibration improves the overall quality and alleviates uncertainty. We apply calibration (‡) to signed GNNs (GPRGNN, FAGCN, and GGCN). We also apply calibration to GCN, GAT, and PTDNet. The average improvements of three signed GNNs by calibration are 4.37%, 3.1%, and 3.13%, respectively. The improvements are greater than those of GCN‡ (2.65%) and GAT‡ (1.97%). Additionally, we describe the dissonance (Eq. 25) of each method in a bracket, where the calibrated methods show lower values than the corresponding vanilla model. To summarize, the results indicate that calibration not only contributes to reducing uncertainty but also improves the accuracy of signed GNNs significantly.

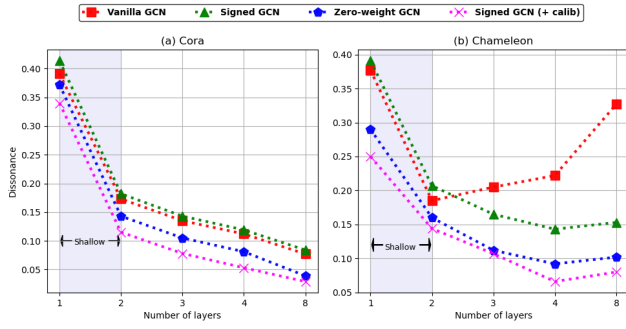


Figure 4: (Q2) Dissonance of four graph variants; vanilla GCN, signed GCN, zero-weight GCN, and signed GCN (+ calib)

6.2 (Q2) Correlation of using signed messages and the uncertainty

To show that signed messages increase uncertainty, we assume three types of graphs for GCN [Kipf and Welling, 2016] using four datasets. Specifically, we fabricate two graph variants, signed GCN and zero-weight GCN. Here, we remove the randomness for a fair comparison. The results are illustrated in Fig. 4, where the x-axis is the number of layers and the y-axis represents dissonance. Referring to Thm. 4.8, the uncertainty is higher on signed GCN for all shallow layers. As we stack more layers, the entropy of vanilla GCN increases dramatically on heterophilous datasets, the Chameleon and Squirrel. In other words, plain GCN fails to discriminate the ego and neighbors (over-smoothing) and yields low classification accuracy.

Table 3: (Q3) Ablation study. We measure the improvement of node classification accuracy (%) by applying edge weight and confidence calibration on three baseline methods, respectively

Datasets	Cora	Citeseer	Actor	Chameleon
GPRGNN	82.2 \pm 0.4	70.4 \pm 0.8	25.4 \pm 0.5	49.1 \pm 0.9
w/ edge calib	83.0 \pm 0.6	71.1 \pm 1.0	25.9 \pm 0.6	49.7 \pm 0.7
w/ conf calib	83.8 \pm 0.5	72.6 \pm 0.5	27.5 \pm 0.4	50.2 \pm 0.3
FAGCN	80.9 \pm 0.5	69.8 \pm 0.6	25.2 \pm 0.8	46.5 \pm 1.1
w/ edge calib	82.1 \pm 0.6	71.6 \pm 0.7	25.8 \pm 0.7	46.9 \pm 1.0
w/ conf calib	83.0 \pm 0.3	72.9 \pm 0.5	26.3 \pm 0.4	48.0 \pm 0.8
GGCN	80.0 \pm 1.2	69.7 \pm 1.6	22.5 \pm 0.5	48.5 \pm 0.7
w/ edge calib	81.9 \pm 1.0	71.0 \pm 1.1	23.3 \pm 0.6	48.9 \pm 0.7
w/ conf calib	82.7 \pm 0.9	72.5 \pm 0.6	23.6 \pm 0.4	49.6 \pm 0.5

6.3 (Q3) Ablation study

We conduct an ablation study to analyze the effectiveness of edge weight and confidence calibration. As shown in Table 3, given the two homophilic (Cora, Citeseer) and heterophilic (Actor, Chameleon) graphs, we employ three baseline methods with signed propagation. For each method, we apply edge weight calibration (**w/ edge calib**) or confidence calibration (**w/ conf calib**) and measure the node classification accuracy, respectively. Here, we can see that methods with confidence calibration generally outperform edge weight calibration and shows smaller variance. The reason is that confidence calibration reduces the uncertainty of the entire nodes

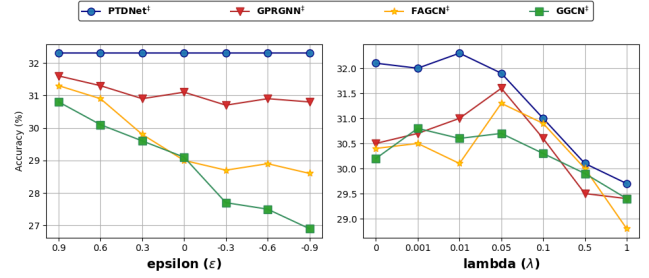


Figure 5: (Q4) The effect of varying hyper-parameter ϵ (left, Eq. 22) and λ (right, Eq. 24) on the classification accuracy, Squirrel dataset

during training, whereas edge calibration is only applied to a small number of edges for testing. Nevertheless, it can also be observed that edge calibration for similar nodes belonging to different classes still contributes to a certain extent to the improvement in performance.

6.4 (Q4) Parameter sensitivity analysis

We conduct an experiment to investigate the effect of hyper-parameter ϵ (Eq. 22) and λ (Eq. 24). We tune the ϵ (threshold of cosine similarity) from -1 to 1 and λ (impact of confidence calibration) from 0 to 1 as shown in Figure 5. Then, we describe the node classification accuracy on the Squirrel (heterophilic) dataset. The blue line represents PTDNet, while others are signed GNNs. In the left figure, we notice that baseline methods achieve the best performance under the largest epsilon, which means blocking the signed messages of highly similar nodes is advantageous (Corollary 4.7). Here, PTDNet does not change the sign of edges, it shows no variation based on the epsilon. In the right figure, it is notable that finding an appropriate lambda is beneficial for overall performance improvement. Nonetheless, it is also limited by the inherent low capability of base models in heterophilous graphs (low accuracy). Further, assigning higher values to the λ generally downgrades the overall performance, which necessitates the usage of validation sets during training.

More experimental results can be found in App. F.

7 Conclusion

In this work, we provide a new theoretical perspective on using signed messages for node embedding under multi-class benchmark datasets. Firstly, we show that signed messages contribute to the separation of heterophilous neighbors in a binary class, which is consistent with conventional studies. Then, we extend previous theorems to a multi-class scenario and point out two critical limitations of using signed propagation: (1) it decreases the separability of two nodes, while (2) increasing the probability of generating conflict evidence. Based on the observations, we calibrate signed GNNs to reduce uncertainty and secure robustness. Through experimental analysis, we show that our method is beneficial for both homophilic and heterophilic graphs. We claim that our theorems can provide insights to develop a better aggregation scheme for future GNN studies.

References

- [Baranwal *et al.*, 2021] Aseem Baranwal, Kimon Fountoulakis, and Aukosh Jagannath. Graph convolution for semi-supervised classification: Improved linear separability and out-of-distribution generalization. *arXiv preprint arXiv:2102.06966*, 2021.
- [Bo *et al.*, 2021] Deyu Bo, Xiao Wang, Chuan Shi, and Huawei Shen. Beyond low-frequency information in graph convolutional networks. *arXiv preprint arXiv:2101.00797*, 2021.
- [Brody *et al.*, 2021] Shaked Brody, Uri Alon, and Eran Yahav. How attentive are graph attention networks? *arXiv preprint arXiv:2105.14491*, 2021.
- [Bruna *et al.*, 2013] Joan Bruna, Wojciech Zaremba, Arthur Szlam, and Yann LeCun. Spectral networks and locally connected networks on graphs. *arXiv preprint arXiv:1312.6203*, 2013.
- [Chen *et al.*, 2020] Ming Chen, Zhewei Wei, Zengfeng Huang, Bolin Ding, and Yaliang Li. Simple and deep graph convolutional networks. In *International Conference on Machine Learning*, pages 1725–1735. PMLR, 2020.
- [Chen *et al.*, 2022] Zhixian Chen, Tengfei Ma, and Yang Wang. When does a spectral graph neural network fail in node classification? *arXiv preprint arXiv:2202.07902*, 2022.
- [Chen *et al.*, 2023] Yuhan Chen, Yihong Luo, Jing Tang, Liang Yang, Siya Qiu, Chuan Wang, and Xiaochun Cao. Lsgnn: Towards general graph neural network in node classification by local similarity. *arXiv preprint arXiv:2305.04225*, 2023.
- [Chien *et al.*, 2020] Eli Chien, Jianhao Peng, Pan Li, and Olga Milenkovic. Adaptive universal generalized pagerank graph neural network. *arXiv preprint arXiv:2006.07988*, 2020.
- [Defferrard *et al.*, 2016] Michaël Defferrard, Xavier Bresson, and Pierre Vandergheynst. Convolutional neural networks on graphs with fast localized spectral filtering. *Advances in neural information processing systems*, 29, 2016.
- [Derr *et al.*, 2018] Tyler Derr, Yao Ma, and Jiliang Tang. Signed graph convolutional networks. In *2018 IEEE International Conference on Data Mining (ICDM)*, pages 929–934. IEEE, 2018.
- [DeVries and Taylor, 2018] Terrance DeVries and Graham W Taylor. Learning confidence for out-of-distribution detection in neural networks. *arXiv preprint arXiv:1802.04865*, 2018.
- [Di Giovanni *et al.*, 2022] Francesco Di Giovanni, James Rowbottom, Benjamin P Chamberlain, Thomas Markovich, and Michael M Bronstein. Graph neural networks as gradient flows. *arXiv preprint arXiv:2206.10991*, 2022.
- [Fang *et al.*, 2022] Zheng Fang, Lingjun Xu, Guojie Song, Qingqing Long, and Yingxue Zhang. Polarized graph neural networks. In *Proceedings of the ACM Web Conference 2022*, pages 1404–1413, 2022.
- [Gilmer *et al.*, 2017] Justin Gilmer, Samuel S Schoenholz, Patrick F Riley, Oriol Vinyals, and George E Dahl. Neural message passing for quantum chemistry. In *International conference on machine learning*, pages 1263–1272. PMLR, 2017.
- [Guo and Wei, 2022] Yuhe Guo and Zhewei Wei. Clenshaw graph neural networks. *arXiv preprint arXiv:2210.16508*, 2022.
- [Guo *et al.*, 2017] Chuan Guo, Geoff Pleiss, Yu Sun, and Kilian Q Weinberger. On calibration of modern neural networks. In *International conference on machine learning*, pages 1321–1330. PMLR, 2017.
- [Huang *et al.*, 2019] Junjie Huang, Huawei Shen, Liang Hou, and Xueqi Cheng. Signed graph attention networks. In *International Conference on Artificial Neural Networks*, pages 566–577. Springer, 2019.
- [Huang *et al.*, 2022] Tiancheng Huang, Donglin Wang, and Yuan Fang. End-to-end open-set semi-supervised node classification with out-of-distribution detection. In *Proceedings of the Thirty-First International Joint Conference on Artificial Intelligence, IJCAI-22*. IJCAI, 2022.
- [Kendall and Gal, 2017] Alex Kendall and Yarin Gal. What uncertainties do we need in bayesian deep learning for computer vision? *Advances in neural information processing systems*, 30, 2017.
- [Kipf and Welling, 2016] Thomas N Kipf and Max Welling. Semi-supervised classification with graph convolutional networks. *arXiv preprint arXiv:1609.02907*, 2016.
- [Klicpera *et al.*, 2018] Johannes Klicpera, Aleksandar Bojchevski, and Stephan Günnemann. Predict then propagate: Graph neural networks meet personalized pagerank. *arXiv preprint arXiv:1810.05997*, 2018.
- [Lei *et al.*, 2022] Runlin Lei, Zhen Wang, Yaliang Li, Bolin Ding, and Zhewei Wei. Evennet: Ignoring odd-hop neighbors improves robustness of graph neural networks. *arXiv preprint arXiv:2205.13892*, 2022.
- [Li *et al.*, 2022] Xiang Li, Renyu Zhu, Yao Cheng, Caihua Shan, Siqiang Luo, Dongsheng Li, and Weining Qian. Finding global homophily in graph neural networks when meeting heterophily. *arXiv preprint arXiv:2205.07308*, 2022.
- [Liu *et al.*, 2021] Meng Liu, Zhengyang Wang, and Shuiwang Ji. Non-local graph neural networks. *IEEE Transactions on Pattern Analysis and Machine Intelligence*, 2021.
- [Liu *et al.*, 2022] Hongrui Liu, Binbin Hu, Xiao Wang, Chuan Shi, Zhiqiang Zhang, and Jun Zhou. Confidence may cheat: Self-training on graph neural networks under distribution shift. In *Proceedings of the ACM Web Conference 2022*, pages 1248–1258, 2022.
- [Luan *et al.*, 2022] Sitao Luan, Chenqing Hua, Qincheng Lu, Jiaqi Zhu, Mingde Zhao, Shuyuan Zhang, Xiao-Wen

- Chang, and Doina Precup. Revisiting heterophily for graph neural networks. *arXiv preprint arXiv:2210.07606*, 2022.
- [Luo *et al.*, 2021] Dongsheng Luo, Wei Cheng, Wenchao Yu, Bo Zong, Jingchao Ni, Haifeng Chen, and Xiang Zhang. Learning to drop: Robust graph neural network via topological denoising. In *Proceedings of the 14th ACM International Conference on Web Search and Data Mining*, pages 779–787, 2021.
- [Ma *et al.*, 2021] Yao Ma, Xiaorui Liu, Neil Shah, and Jiliang Tang. Is homophily a necessity for graph neural networks? *arXiv preprint arXiv:2106.06134*, 2021.
- [McPherson *et al.*, 2001] Miller McPherson, Lynn Smith-Lovin, and James M Cook. Birds of a feather: Homophily in social networks. *Annual review of sociology*, pages 415–444, 2001.
- [Moon *et al.*, 2020] Jooyoung Moon, Jiho Kim, Younghak Shin, and Sangheum Hwang. Confidence-aware learning for deep neural networks. In *international conference on machine learning*, pages 7034–7044. PMLR, 2020.
- [Mukherjee and Awadallah, 2020] Subhabrata Mukherjee and Ahmed Awadallah. Uncertainty-aware self-training for few-shot text classification. *Advances in Neural Information Processing Systems*, 33:21199–21212, 2020.
- [Nt and Maehara, 2019] Hoang Nt and Takanori Maehara. Revisiting graph neural networks: All we have is low-pass filters. *arXiv preprint arXiv:1905.09550*, 2019.
- [Oono and Suzuki, 2019] Kenta Oono and Taiji Suzuki. Graph neural networks exponentially lose expressive power for node classification. *arXiv preprint arXiv:1905.10947*, 2019.
- [Pei *et al.*, 2020] Hongbin Pei, Bingzhe Wei, Kevin Chen-Chuan Chang, Yu Lei, and Bo Yang. Geom-gcn: Geometric graph convolutional networks. *arXiv preprint arXiv:2002.05287*, 2020.
- [Perry, 2013] Chris Perry. Machine learning and conflict prediction: a use case. *Stability: International Journal of Security and Development*, 2(3):56, 2013.
- [Platonov *et al.*, 2023] Oleg Platonov, Denis Kuznedelev, Michael Diskin, Artem Babenko, and Liudmila Prokhorenkova. A critical look at the evaluation of gnn under heterophily: are we really making progress? *arXiv preprint arXiv:2302.11640*, 2023.
- [Rozemberczki *et al.*, 2019] Benedek Rozemberczki, Ryan Davies, Rik Sarkar, and Charles Sutton. Gemsec: Graph embedding with self clustering. In *Proceedings of the 2019 IEEE/ACM international conference on advances in social networks analysis and mining*, pages 65–72, 2019.
- [Shannon, 1948] Claude Elwood Shannon. A mathematical theory of communication. *The Bell system technical journal*, 27(3):379–423, 1948.
- [Sun *et al.*, 2022] Yifei Sun, Haoran Deng, Yang Yang, Chunping Wang, Jiarong Xu, Renhong Huang, Linfeng Cao, Yang Wang, and Lei Chen. Beyond homophily: Structure-aware path aggregation graph neural network. In Lud De Raedt, editor, *Proceedings of the Thirty-First International Joint Conference on Artificial Intelligence, IJCAI-22*, pages 2233–2240. International Joint Conferences on Artificial Intelligence Organization, 7 2022. Main Track.
- [Tang *et al.*, 2009] Jie Tang, Jimeng Sun, Chi Wang, and Zi Yang. Social influence analysis in large-scale networks. In *Proceedings of the 15th ACM SIGKDD international conference on Knowledge discovery and data mining*, pages 807–816, 2009.
- [Velickovic *et al.*, 2017] Petar Velickovic, Guillem Cucurull, Arantxa Casanova, Adriana Romero, Pietro Lio, and Yoshua Bengio. Graph attention networks. *stat*, 1050:20, 2017.
- [Wang and Zhang, 2022] Xiyuan Wang and Muhan Zhang. How powerful are spectral graph neural networks. In *International Conference on Machine Learning*, pages 23341–23362. PMLR, 2022.
- [Wang *et al.*, 2021] Xiao Wang, Hongrui Liu, Chuan Shi, and Cheng Yang. Be confident! towards trustworthy graph neural networks via confidence calibration. *Advances in Neural Information Processing Systems*, 34:23768–23779, 2021.
- [Wang *et al.*, 2022] Tao Wang, Di Jin, Rui Wang, Dongxiao He, and Yuxiao Huang. Powerful graph convolutional networks with adaptive propagation mechanism for homophily and heterophily. In *Proceedings of the AAAI Conference on Artificial Intelligence*, volume 36, pages 4210–4218, 2022.
- [Yan *et al.*, 2021] Yujun Yan, Milad Hashemi, Kevin Swersky, Yaoqing Yang, and Danai Koutra. Two sides of the same coin: Heterophily and oversmoothing in graph convolutional neural networks. *arXiv preprint arXiv:2102.06462*, 2021.
- [Yang *et al.*, 2021] Han Yang, Kaili Ma, and James Cheng. Rethinking graph regularization for graph neural networks. In *Proceedings of the AAAI Conference on Artificial Intelligence*, volume 35, pages 4573–4581, 2021.
- [Zhao *et al.*, 2020] Xujiang Zhao, Feng Chen, Shu Hu, and Jin-Hee Cho. Uncertainty aware semi-supervised learning on graph data. *Advances in Neural Information Processing Systems*, 33:12827–12836, 2020.
- [Zhu *et al.*, 2020] Jiong Zhu, Yujun Yan, Lingxiao Zhao, Mark Heimann, Leman Akoglu, and Danai Koutra. Beyond homophily in graph neural networks: Current limitations and effective designs. *Advances in Neural Information Processing Systems*, 33:7793–7804, 2020.
- [Zhu *et al.*, 2021] Jiong Zhu, Ryan A Rossi, Anup Rao, Tung Mai, Nedim Lipka, Nesreen K Ahmed, and Danai Koutra. Graph neural networks with heterophily. In *Proceedings of the AAAI Conference on Artificial Intelligence*, volume 35, pages 11168–11176, 2021.

Technical Appendix

A. Proof of Theorem 4.1, 4.2, 4.3 and Equation 13

A.1. Proof of Theorem 4.1. [Binary class, vanilla GCN [Yan *et al.*, 2021]]

A detailed proof of Theorem 4.1 and 4.2 is provided in [Yan *et al.*, 2021], where we introduce them briefly here. Assume a binary class $y_i \in \{0, 1\}$. Using the aggregation scheme of GCN [Kipf and Welling, 2016], the hidden representation of node i after message-passing $h_i^{(1)}$ is defined as:

$$h_i^{(1)} = \frac{h_i^{(0)}}{d_i + 1} + \sum_{j \in \mathcal{N}_i} \frac{h_j^{(0)}}{\sqrt{(d_i + 1)(d_j + 1)}} \quad (26)$$

As illustrated in Figure 6a (binary class), we assume $h_i \sim N(\mu, \frac{1}{\sqrt{d_i}})$ if $y_i = 0$ and otherwise $h_i \sim N(-\mu, \frac{1}{\sqrt{d_i}})$. Based on the local homophily ratio b_i , Eq. 26 can be extended as:

$$\begin{aligned} \mathbb{E}(h_i^{(1)} | v_i, d_i) &= \frac{\mu}{d_i + 1} + \sum_{j \in \mathcal{N}_i} \left(\frac{b_i}{\sqrt{(d_i + 1)(d_j + 1)}} \mu - \frac{(1 - b_i)}{\sqrt{(d_i + 1)(d_j + 1)}} \mu \right) \\ &= \left(\frac{1}{d_i + 1} + \sum_{j \in \mathcal{N}_i} \frac{2b_i - 1}{\sqrt{(d_i + 1)(d_j + 1)}} \right) \mu \\ &= \left(\frac{1}{d_i + 1} + \frac{2b_i - 1}{d_i + 1} \sum_{j \in \mathcal{N}_i} \frac{\sqrt{d_i + 1}}{\sqrt{d_j + 1}} \right) \mu \\ &= \left(\frac{1 + (2b_i - 1)d'_i}{d_i + 1} \right) \mu. \end{aligned} \quad (27)$$

A.2. Proof of Theorem 4.2. [Binary class, signed GCN [Yan *et al.*, 2021]]

Similarly, signed GCN correctly configures the sign of heterophilous edges with the following error ratio $1 - e$. For example, the sign of heterophilous nodes changes from $-\mu$ to μ with a probability $1 - e$ and vice versa:

$$\begin{aligned} \mathbb{E}(h_i^{(1)} | v_i, d_i) &= \frac{\mu}{d_i + 1} + \sum_{j \in \mathcal{N}_i} \left(\frac{\mu(1 - e) - \mu e}{\sqrt{(d_i + 1)(d_j + 1)}} b_i + \frac{\mu(1 - e) - \mu e}{\sqrt{(d_i + 1)(d_j + 1)}} (1 - b_i) \right) \\ &= \frac{\mu}{d_i + 1} + \sum_{j \in \mathcal{N}_i} \left(\frac{1 - 2e}{\sqrt{(d_i + 1)(d_j + 1)}} \mu \right) \\ &= \left(\frac{1}{d_i + 1} + \frac{1 - 2e}{d_i + 1} \sum_{j \in \mathcal{N}_i} \frac{\sqrt{d_i + 1}}{\sqrt{d_j + 1}} \right) \mu \\ &= \left(\frac{1 + (1 - 2e)d'_i}{d_i + 1} \right) \mu. \end{aligned} \quad (28)$$

A.3. Proof of Theorem 4.3. [Binary class, zero-weight GCN]

Likewise, we can induce the expectation of zero-weight GCN by assigning zero weights on heterophilous nodes as follows:

$$\begin{aligned} \mathbb{E}(h_i^{(1)} | v_i, d_i) &= \frac{\mu}{d_i + 1} + \sum_{j \in \mathcal{N}_i} \left(\frac{\mu(1 - e) - \mu e \times 0}{\sqrt{(d_i + 1)(d_j + 1)}} b_i + \frac{\mu(1 - e) \times 0 - \mu e}{\sqrt{(d_i + 1)(d_j + 1)}} (1 - b_i) \right) \\ &= \frac{\mu}{d_i + 1} + \sum_{j \in \mathcal{N}_i} \left(\frac{b_i - e}{\sqrt{(d_i + 1)(d_j + 1)}} \mu \right) \\ &= \left(\frac{1}{d_i + 1} + \frac{b_i - e}{d_i + 1} \sum_{j \in \mathcal{N}_i} \frac{\sqrt{d_i + 1}}{\sqrt{d_j + 1}} \right) \mu \\ &= \left(\frac{1 + (b_i - e)d'_i}{d_i + 1} \right) \mu. \end{aligned} \quad (29)$$

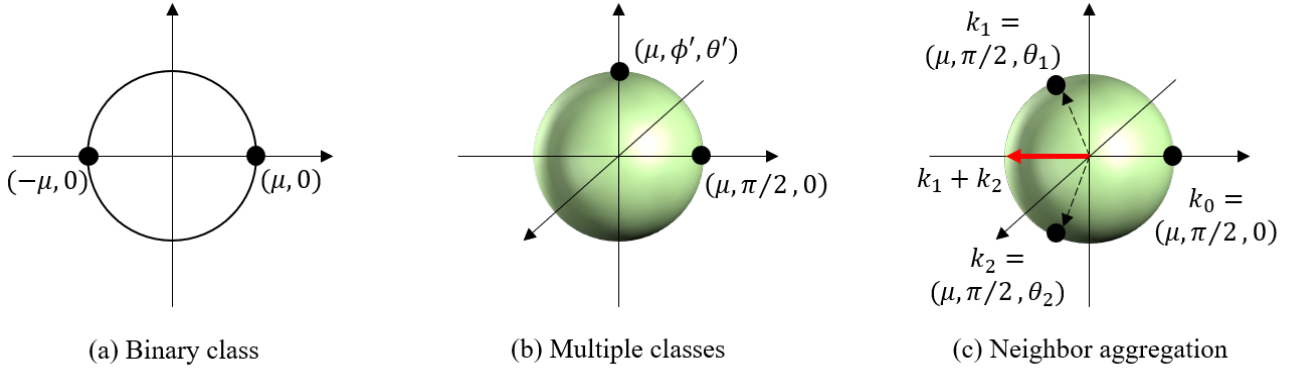


Figure 6: We take an example to illustrate the distribution of node features under (a) binary and (b) multi-class scenarios. Figure (c) represents the aggregation of neighboring nodes (k_1, k_2) under multiple classes

A.4. Proof of Equation 13

We first show that signed messages can contribute to separating the ego from its neighbors. Let us assume the label of the ego node i is k . A neighbor node j is connected to i with a signed edge. Since the column-wise components of the weight matrix act as an independent classifier, the probabilities that the two nodes belong to the same class k , $\hat{y}_{i,k}, \hat{y}_{j,k}$, at a training epoch t are derived as,

$$\begin{aligned}\hat{y}_{i,k}^{(t+1)} &= \hat{y}_{i,k}^t - \eta \nabla_i \mathcal{L}_{nll}(Y_i, \hat{Y}_i)_k \\ \hat{y}_{j,k}^{(t+1)} &= \hat{y}_{j,k}^t - \eta \nabla_j \mathcal{L}_{nll}(Y_i, \hat{Y}_i)_k\end{aligned}\tag{30}$$

The loss function is defined as $\mathcal{L}_{nll}(Y_i, \hat{Y}_i)_k = -\log(\hat{y}_{i,k})$, where $\hat{Y}_i = \sigma(\bar{H}_i^L) = \sigma(\frac{\bar{H}_i^{(L)}}{d_i+1} - \frac{\bar{H}_j^{(L)}}{\sqrt{(d_i+1)(d_j+1)}})$. The gradient $\nabla_i \mathcal{L}_{nll}(Y_i, \hat{Y}_i)_k$ is well-known to be,

$$\begin{aligned}\nabla_i \mathcal{L}_{nll}(Y_i, \hat{Y}_i)_k &= \frac{\partial \mathcal{L}_{nll}(Y_i, \hat{Y}_i)_k}{\partial \hat{y}_{i,k}} = \frac{\partial \mathcal{L}_{nll}(Y_i, \hat{Y}_i)_k}{\partial \hat{y}_{i,k}} \cdot \frac{\partial \hat{y}_{i,k}}{\partial h_{i,k}^{(L)}} \\ &= -\frac{1}{\hat{y}_{i,k}} \cdot (\hat{y}_{i,k}(1 - \hat{y}_{i,k})) = \hat{y}_{i,k} - 1 < 0\end{aligned}\tag{31}$$

Similarly, the gradient $\nabla_j \mathcal{L}_{nll}(Y_i, \hat{Y}_i)_k$ is given by:

$$\begin{aligned}\nabla_j \mathcal{L}_{nll}(Y_i, \hat{Y}_i)_k &= \frac{\partial \mathcal{L}_{nll}(Y_i, \hat{Y}_i)_k}{\partial \hat{y}_{i,k}} = \frac{\partial \mathcal{L}_{nll}(Y_i, \hat{Y}_i)_k}{\partial \hat{y}_{i,k}} \cdot \frac{\partial \hat{y}_{i,k}}{\partial h_{j,k}^{(L)}} \\ &= -\frac{1}{\hat{y}_{i,k}} \cdot (\hat{y}_{i,k}(1 - \hat{y}_{i,k})(-1)) = 1 - \hat{y}_{i,k} > 0,\end{aligned}\tag{32}$$

where we can infer that $\hat{y}_{i,k}^{(t+1)} > \hat{y}_{i,k}^t$ and $\hat{y}_{j,k}^{(t+1)} < \hat{y}_{j,k}^t$.

B. Proof of Theorem 4.5, 4.6, and Corollary 4.7

B.1. Proof of Theorem 4.5. [Multi-class, signed GCN]

As shown in Figure 6b, we extend a binary classification scenario to a multi-class case. Without loss of generality, we employ spherical coordinates and ensure that μ corresponds to the scale of a vector, while the direction of each vector lies between zero and ϕ, θ with respect to their features. Here, we assume the label is $y_i = 0$. For simplicity, we replace $(\mu, \phi = \pi/2, \theta = 0)$ as k and (μ, ϕ', θ') as k' , respectively. Though k' comprises multiple distributions that are proportional to the number of classes, their aggregation always satisfies $|k'_{aggr}| \leq \mu$ since the summation of coefficients $(1 - b_i)$ is lower than 1 and $|k'| \leq \mu$. Referring to Fig. 6c, we can see that $\frac{k_1+k_2}{2} \leq \mu$ given $b_1 = b_2 = 0.5$, where the aggregation of neighbors always lies in μ .

Thus, for brevity, we indicate k'_{aggr} as k' here. Now, we can retrieve the expectation (h_i) of signed GCN as follows:

$$\begin{aligned}
\mathbb{E}(h_i^{(1)}|v_i, d_i) &= \frac{k}{d_i + 1} + \sum_{j \in \mathcal{N}_i} \left(\frac{k(1-e) - ke}{\sqrt{(d_i + 1)(d_j + 1)}} b_i + \frac{-k'(1-e) + k'e}{\sqrt{(d_i + 1)(d_j + 1)}} (1 - b_i) \right) \\
&= \frac{k}{d_i + 1} + \sum_{j \in \mathcal{N}_i} \left(\frac{k(1-2e)b_i - k'(1-2e)(1-b_i)}{\sqrt{(d_i + 1)(d_j + 1)}} \right) \\
&= \frac{k}{d_i + 1} + \sum_{j \in \mathcal{N}_i} \left(\frac{(1-2e)\{kb_i + k'(b_i - 1)\}}{\sqrt{(d_i + 1)(d_j + 1)}} \right) \\
&= \frac{k}{d_i + 1} + \frac{(1-2e)\{kb_i + k'(b_i - 1)\}d'}{d_i + 1} \\
&= \frac{(1-2e)\{b_i k + (b_i - 1)k'\}d'_i + k}{d_i + 1}.
\end{aligned} \tag{33}$$

B.2. Proof of Theorem 4.6. [Multi-class, zero-weight GCN]

Similar to Eq. 33, the expectation of assigning zero weights for multi-class GCN is given by:

$$\begin{aligned}
\mathbb{E}(h_i^{(1)}|v_i, d_i) &= \frac{k}{d_i + 1} + \sum_{j \in \mathcal{N}_i} \left(\frac{k(1-e) - ke \times 0}{\sqrt{(d_i + 1)(d_j + 1)}} b_i + \frac{k'(1-e) \times 0 + k'e}{\sqrt{(d_i + 1)(d_j + 1)}} (1 - b_i) \right) \\
&= \frac{k}{d_i + 1} + \sum_{j \in \mathcal{N}_i} \left(\frac{k(1-e)b_i + k'e(1-b_i)}{\sqrt{(d_i + 1)(d_j + 1)}} \right) \\
&= \frac{k}{d_i + 1} + \frac{\{(1-e)b_i k + e(1-b_i)k'\}d'_i}{d_i + 1} \\
&= \frac{\{(1-e)b_i k + e(1-b_i)k'\}d'_i + k}{d_i + 1}.
\end{aligned} \tag{34}$$

B.3. Analysis on Corollary 4.7

Taking Eq. 33 and 34, one can compare the discrimination power between a sign-flip and zero-weight GCN under a multi-class scenario. Exclude the overlapping part $\frac{k}{d_i + 1}$, Z can be retrieved as below:

$$\begin{aligned}
Z &= (1-2e)\{b_i k + (b_i - 1)k'\} - \{(1-e)b_i k + e(1-b_i)k'\} \\
&= -eb_i k + (1-e)(b_i - 1)k'
\end{aligned} \tag{35}$$

As mentioned above, $k' = (\mu', \theta')$ where $0 \leq \mu' \leq \mu$ and $0 \leq \theta' \leq 2\pi$. If the scale of the aggregated vector is $|\mu'| = 0$, $Z = -eb_i k \leq 0$ and this implies zero-weight GCN generally outperforms signed GCN. Instead, assuming the scale as $\mu' = \mu$, Z is determined w.r.t. the angle of k' as follows:

$$Z \in \begin{cases} 1 - e - b, & \text{if } k' = -k \\ -2eb - (1 - e - b), & \text{if } k' = k, \end{cases} \tag{36}$$

Firstly, if k' is origin symmetric to k , the plane Z is half-divided as,

$$\int_0^1 \int_0^1 (1 - e - b) dedb = \left[1 - \frac{e^2 + b^2}{2} \right]_{e,b=0}^1 = 0 \tag{37}$$

However, as k' gets closer to k , we notice that Z tends to be negative as below:

$$\int_0^1 \int_0^1 (-2eb + e + b - 1) dedb = \left[\frac{-eb^2 - e^2b + e^2 + b^2}{2} - 1 \right]_{e,b=0}^1 = -1. \tag{38}$$

Intuitively, the probability of being $k' = -k$ is inversely proportional to the number of entire classes. Thus, one can infer that zero-weight GCN generally outperforms signed one given multi-class datasets.

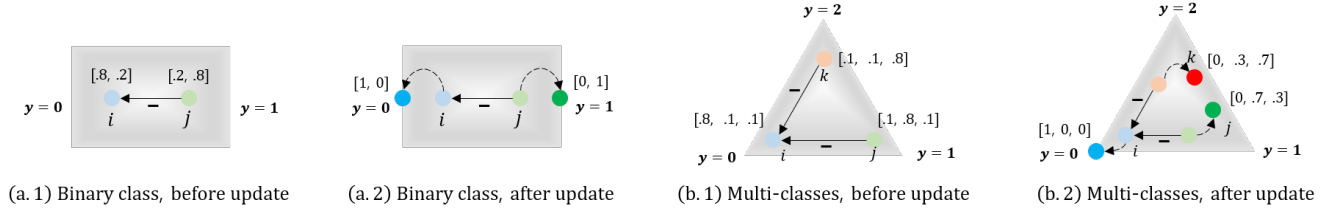


Figure 7: We visualize the update procedure of node features under (a) binary and (b) multi-class scenarios through Dirichlet distribution

C. Proof of Theorem 4.8

In § A.1., we proved that signed messages contribute to the separation of ego and neighbors as below:

$$\begin{aligned}\hat{y}_{i,k}^{(t+1)} &= \hat{y}_{i,k}^t - \eta \nabla_i \mathcal{L}_{nll}(Y_i, \hat{Y}_i)_k > \hat{y}_{i,k}^t, \\ \hat{y}_{j,k}^{(t+1)} &= \hat{y}_{j,k}^t - \eta \nabla_j \mathcal{L}_{nll}(Y_i, \hat{Y}_i)_k < \hat{y}_{j,k}^t,\end{aligned}\quad (39)$$

in case the label of ego (i) is k , and the neighboring node (j) is connected with a signed edge.

Here, let us assume two nodes s and p , which are connected to a central node i with a signed (s) and plane edge (p), respectively. We aim to show that a difference between the $E(\hat{y}_s)$ and $E(\hat{y}_p)$ increases w.r.t. the training epoch (t) under a multi-class scenario:

$$E(\hat{y}_s^{(t+1)}) - E(\hat{y}_p^{(t+1)}) > E(\hat{y}_s^t) - E(\hat{y}_p^t). \quad (40)$$

Firstly, the true label probability (k) of node p $\hat{y}_{p,k}$ increases, while other probabilities $\hat{y}_{p,o}$ ($o \neq k$) decrease as follows:

$$\hat{y}_p^{(t+1)} \in \begin{cases} \hat{y}_{p,k}^t - \eta \nabla_p \mathcal{L}_{nll}(Y_i, \hat{Y}_i)_k > \hat{y}_{p,k}^t, \\ \hat{y}_{p,o}^t - \eta \nabla_p \mathcal{L}_{nll}(Y_i, \hat{Y}_i)_o < \hat{y}_{p,o}^t, \quad \forall o \neq k. \end{cases} \quad (41)$$

Since we proved that $\nabla_p \mathcal{L}_{nll}(Y_i, \hat{Y}_i)_k < 0$ in Eq. 31, we analyze the partial derivative $\nabla_p \mathcal{L}_{nll}(Y_i, \hat{Y}_i)_o$ ($\forall o \neq k$):

$$\begin{aligned}\nabla_p \mathcal{L}_{nll}(Y_i, \hat{Y}_i)_o &= \frac{\partial \mathcal{L}_{nll}(Y_i, \hat{Y}_i)_o}{\partial \hat{y}_{p,o}} = \frac{\partial \mathcal{L}_{nll}(Y_i, \hat{Y}_i)_o}{\partial \hat{y}_{i,o}} \cdot \frac{\partial \hat{y}_{i,o}}{\partial \hat{h}_{p,o}^{(L)}} \\ &= \frac{1}{\hat{y}_{i,o}} \cdot (\hat{y}_{i,o}(1 - \hat{y}_{i,o})) = 1 - \hat{y}_{i,o} > 0,\end{aligned}\quad (42)$$

which satisfies $\hat{y}_{p,o}^t - \eta \nabla_p \mathcal{L}_{nll}(Y_i, \hat{Y}_i)_o < \hat{y}_{p,o}^t$.

On the contrary, the gradient of node s has a different sign with node p , where we can infer that:

$$\hat{y}_s^{(t+1)} \in \begin{cases} \hat{y}_{s,k}^t - \eta \nabla_s \mathcal{L}_{nll}(Y_i, \hat{Y}_i)_k < \hat{y}_{s,k}^t, \\ \hat{y}_{s,o}^t - \eta \nabla_s \mathcal{L}_{nll}(Y_i, \hat{Y}_i)_o > \hat{y}_{s,o}^t, \quad \forall o \neq k. \end{cases} \quad (43)$$

As the training epoch increases, $\hat{y}_{p,k}$ will converge to 1 resulting in the decrease of $E(\hat{y}_p)$. Conversely, $\hat{y}_{s,k}$ gets closer to 0, which may fail to generate a highly confident prediction and leads to a surge of uncertainty. Thus, one can infer that $E(\hat{y}_s^{(t+1)}) - E(\hat{y}_p^{(t+1)}) > E(\hat{y}_s^t) - E(\hat{y}_p^t)$ as $t \rightarrow \infty$. As shown in Figure 7a, this can be effective under a binary class, while the signed nodes (i, j) in a multi-class case (Fig. 7b) have conflict evidence except for class 0. Taking another example, let us assume that the original probability (before the update) is $\hat{y}_i^t = [0.6, 0.2, 0.2]$ with $C = 3$. Then, one can calculate the Shannon's entropy (E) of \hat{y}_i^t as,

$$E(\hat{y}_i^t) = - \sum_{j=1}^3 \hat{y}_{i,j}^t \log_3 \hat{y}_{i,j}^t \approx 0.8649 \quad (44)$$

Without considering node degree, let us assume the gradient of class k as $\nabla_p \mathcal{L}_{nll}(Y_i, \hat{Y}_i)_k = -\nabla_s \mathcal{L}_{nll}(Y_i, \hat{Y}_i)_k = \alpha$, and other classes as $\nabla_p \mathcal{L}_{nll}(Y_i, \hat{Y}_i)_o = -\nabla_s \mathcal{L}_{nll}(Y_i, \hat{Y}_i)_o = \frac{\alpha}{C-1}$ ($\forall o \neq k$). If we take $\alpha = 0.1$, $\hat{y}_p^{(t+1)}$ and $\hat{y}_s^{(t+1)}$ becomes:

$$E(\hat{y}_p^{(t+1)}) = E([0.8, 0.1, 0.1]) \approx 0.5817, \quad E(\hat{y}_s^{(t+1)}) = E([0.4, 0.3, 0.3]) \approx 0.9911, \quad (45)$$

where we can see that $E(\hat{y}_p^{(t+1)}) < E(\hat{y}_s^{(t+1)})$ after the single iteration.

D. Pseudo-code and Time Complexity of Our Algorithm

D.1. The pseudo-code of calibrated FAGCN [Bo *et al.*, 2021] is as below. Instead of FAGCN, any type of GNNs can be integrated with our method

Algorithm 1 Pseudo-code of calibrated FAGCN

Require: Adjacency matrix (A), initial node features (X), node embedding at l^{th} layer (H^l), attention weight between two nodes (a_{ij}), initialized parameters of FAGCN (θ), edge weight threshold (ϵ), best validation score ($\alpha^* = 0$)

Ensure: Parameters with the best validation score (θ^*)

```

1: for training epochs do
2:   # Training (forward pass with confidence calibration)
3:   Retrieve class probability through forward pass,  $\hat{Y} = \sigma(\bar{H}^{(L)})$ 
4:   Compute negative-log likelihood loss,  $\mathcal{L}_{FAGCN} = \mathcal{L}_{nll}(Y, \hat{Y})$ 
5:   Compute calibration loss,  $\mathcal{L}_{conf} = \frac{1}{n} \sum_{i=1}^n (-\max(\hat{y}_i) + \text{submax}(\hat{y}_i))$ ,  $n = |\mathcal{V}_{valid} \cup \mathcal{V}_{test}|$ 
6:   Get total loss,  $\mathcal{L}_{total} = \mathcal{L}_{FAGCN} + \lambda \mathcal{L}_{conf}$ 
7:   Update parameters,  $\theta' = \theta - \eta \frac{\partial \mathcal{L}_{total}}{\partial \theta}$ 
8:   # Validation (forward pass with edge weight calibration)
9:   Retrieve  $l^{th}$  layer's node embedding,  $H^l$ 
10:  Get node  $i$ 's embedding,  $h_i^l$ 
11:  Get attention weights  $a_{ij}$  of adjacent nodes ( $j$ ),  $a_{ij} = \tanh(g^T [h_i^l || h_j^l])$  *  $g^T$ : learnable vector
12:  Calculate cosine similarity,  $\cos(h_i^l, h_j^l) = \frac{h_i^l \cdot h_j^l}{\|h_i^l\|_2 \|h_j^l\|_2}$ 
13:  if  $a_{ij} < 0 \wedge \cos(h_i^l, h_j^l) > \epsilon$ , then
14:    Replace  $a_{ij}$  as 0
15:  Using the updated parameters ( $\theta'$ ) and calibrated attention weights ( $a_{ij}$ ), get validation score  $\alpha$ 
16:  if  $\alpha > \alpha^*$  then
17:    Save current parameters,  $\theta^* = \theta'$ 
18:    Update best validation score,  $\alpha^* = \alpha$ 

```

D.2. Time complexity of calibrated GNN

We analyze the computational complexity of calibrated GNN. For brevity, we take vanilla GCN [Kipf and Welling, 2016] as a base model. Generally, the cost of GCN is known to be proportional to the number of edges and trainable parameters $\mathcal{O}(|\mathcal{E}| \theta_{GCN})$. Here, θ_{GCN} is comprised of $\mathcal{O}(nz(X)F' + F'C)$ [Zhu *et al.*, 2020], where $nz(\cdot)$ represents the non-zero elements of inputs and F' stand for the hidden dimension, and C is the number of classes. Additionally, our method employs two types of calibration. The first one is edge weight calibration. For this, we need to retrieve the node features of each layer and calculate the cosine similarity for all connected nodes $|\mathcal{E}|^2$. Thus, the complexity becomes $\mathcal{O}(|\mathcal{E}| \theta_{GCN} + L|\mathcal{E}|^2)$, where L represents the number of entire layers. Additionally, confidence calibration takes $n = |\mathcal{V}_{valid} \cup \mathcal{V}_{test}|$ samples as inputs and finds top k samples on each row of \hat{Y} . Thus, their complexity can be simply defined as $\mathcal{O}(n + k)$. To summarize, the cost of calibrated GCN is $\mathcal{O}(2|\mathcal{E}| \theta_{GCN} + L|\mathcal{E}|^2 + n + k)$, which is fairly efficient compared to plane algorithm.

E. Implementations Details

E.1. General information

All methods including baselines and ours are implemented upon *PyTorch Geometric*¹. For a fair comparison, we equalize the hidden dimension of the entire methodologies as 64. ReLU with dropout is used for non-linearity and to prevent over-fitting. We employ the log-Softmax as a cross-entropy function. The learning ratio is set to $1e^{-3}$ and the Adam optimizer is taken with weight decay $5e^{-4}$. For training, 20 nodes per class are randomly chosen and the remaining nodes are equally divided into two

¹<https://pytorch-geometric.readthedocs.io/en/latest/modules/nn.html>

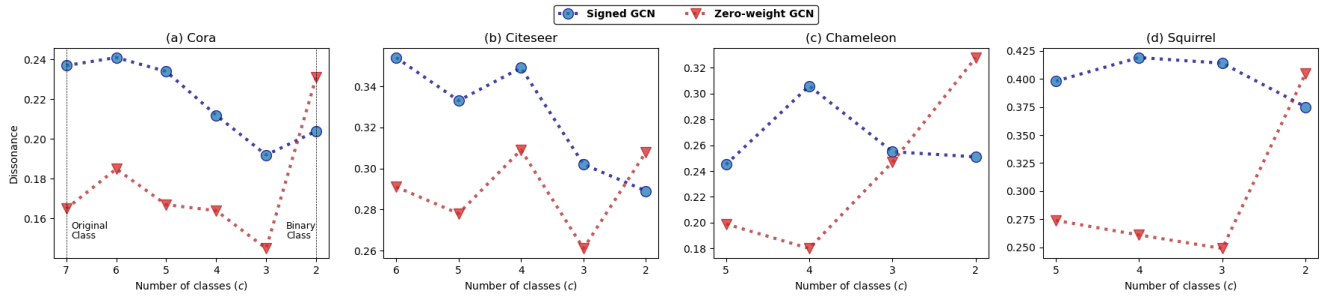


Figure 8: By differentiating the number of classes, we compare the dissonance of signed GCN and zero-weight GCN using two graph variants. The leftmost value on the x-axis represents the original class, and the rightmost value represents the binary class

parts for validation and testing.

E.2. Implementation details about baseline methods

- **GCN** [Kipf and Welling, 2016] is a first-order approximation of Chebyshev polynomials [Defferrard *et al.*, 2016]. For all datasets, we simply take 2 layers of GCN.
- **APNP** [Klicpera *et al.*, 2018] combines personalized PageRank on GCN. We stack 10 layers and set the teleport probability (α) as $\{0.1, 0.1, 0.1, 0.5, 0.2, 0.3\}$ for Cora, Citeseer, Pubmed, Actor, Chameleon, and Squirrel.
- **GAT** [Velickovic *et al.*, 2017] calculates feature-based attention for edge coefficients. Similar to GCN, we construct 2 layers of GAT. The pair of (hidden dimension, head) is set as (8, 8) for the first layer, while the second layer is (1, number of classes).
- **GCNII** [Chen *et al.*, 2020] integrates an identity mapping function on APNP. We set $\alpha = 0.5$ and employ nine hidden layers. We increase the weight of identity mapping (β) that is inversely proportional to the heterophily of the dataset.
- **H₂GCN** [Zhu *et al.*, 2020] suggests the separation of ego and neighbors during aggregation. We refer to the publicly available *source code*² for implementation.
- **PTDNet** [Luo *et al.*, 2021] removes disassortative edges before a message-passing. We also utilize the open *source code*³ here.
- **GPRGNN** [Chien *et al.*, 2020] generalized the personalized PageRank to deal with heterophily and over-smoothing. Referring to the open *source code*⁴, we tune the hyper-parameters based on the best validation score for each dataset.
- **FAGCN** [Bo *et al.*, 2021] determines the sign of edges using the node features. We implement the algorithm based on the *sources*⁵ and tune the hyper-parameters with respect to their accuracy.
- **GGCN** [Yan *et al.*, 2021] proposes the scaling of degrees and the separation of positive/negative adjacency matrices. We simply take the publicly available *code*⁶ for evaluation.

F. Further Evaluation

F.1. Case study

Through theoretical analyses (§ 4.4), we confirm that signed messages increase the uncertainty in multi-class graphs. They have shown to be effective when k' gets closer to $-k$ (Eq. 18), but this probability is inversely proportional to the number of classes c . To further analyze this phenomenon, we compare the dissonance of two variants of GCN (signed GCN and zero-weight GCN) by decrement of the number of classes (c). Specifically, if the original data contains seven classes (e.g., Cora), we remove all the nodes that belong to the rightmost class to generate a graph with six labels. The results are illustrated in Figure 8. As can be seen, zero-weight GCN (red) tends to have lower dissonance under multiple classes. However, under binary classes ($c=2$), signed GCN (blue) shows lower uncertainty with the aid of ego-neighbor separation. In the binary case, zero-weight GCN only utilizes homophilous neighbors and fails to generalize under this condition.

²<https://github.com/GemsLab/H2GCN>

³<https://github.com/flyingdoog/PTDNet>

⁴<https://github.com/jianhao2016/GPRGNN>

⁵<https://github.com/bdy9527/FAGCN>

⁶https://github.com/Yujun-Yan/Heterophily_and_oversmoothing

Table 4: Node classification accuracy (%) on nine benchmark graphs. The gray-colored cell means the top 3 and bold with (*) indicates the best performances. Symbol ‡ means that calibration is applied to the baseline method

Datasets	Cora	Citeseer	Pubmed	Actor	Chameleon	Squirrel	Cornell	Texas	Wisconsin
\mathcal{H}_g (Eq. 1)	0.81	0.74	0.8	0.22	0.23	0.22	0.11	0.06	0.16
MLP	53.2 \pm 0.5	53.7 \pm 1.7	69.7 \pm 0.4	27.9* \pm 1.1	41.2 \pm 1.8	26.5 \pm 0.6	60.1 \pm 1.2	65.8 \pm 5.0	73.5* \pm 5.4
GCN	79.0 \pm 0.6	67.5 \pm 0.8	77.6 \pm 0.2	20.2 \pm 0.4	49.3 \pm 0.5	31.7 \pm 0.7	39.4 \pm 4.3	47.6 \pm 0.7	40.5 \pm 1.9
GCN ‡	81.0 \pm 0.9	71.3 \pm 1.2	77.8 \pm 0.4	21.7 \pm 0.6	49.4 \pm 0.6	31.5 \pm 0.6	39.6 \pm 3.1	48.0 \pm 0.6	40.5 \pm 1.4
GAT	80.1 \pm 0.6	68.0 \pm 0.7	78.0 \pm 0.4	22.5 \pm 0.3	47.9 \pm 0.8	30.8 \pm 0.9	42.1 \pm 3.1	49.2 \pm 4.4	45.8 \pm 5.3
GAT ‡	81.4 \pm 0.4	72.2 \pm 0.6	78.3 \pm 0.3	23.2 \pm 1.8	49.2 \pm 0.4	30.3 \pm 0.8	42.5 \pm 2.5	49.3 \pm 4.1	47.1 \pm 5.0
GATv2	79.5 \pm 0.5	67.4 \pm 0.6	76.2 \pm 0.5	22.1 \pm 2.0	48.3 \pm 0.4	28.9 \pm 1.2	38.0 \pm 3.8	52.5 \pm 1.7	41.7 \pm 5.1
GIN	77.3 \pm 0.8	66.1 \pm 0.6	77.1 \pm 0.7	24.6 \pm 0.8	49.1 \pm 0.7	28.4 \pm 2.2	42.9 \pm 4.6	53.5 \pm 3.0	38.2 \pm 1.5
APPNP	81.3 \pm 0.5	68.9 \pm 0.3	79.0 \pm 0.3	23.8 \pm 0.3	48.0 \pm 0.7	30.4 \pm 0.6	49.8 \pm 3.6	56.1 \pm 0.2	45.7 \pm 1.7
GCNII	81.1 \pm 0.7	68.5 \pm 1.4	78.5 \pm 0.4	25.9 \pm 1.2	48.1 \pm 0.7	29.1 \pm 0.9	62.5 \pm 0.5	69.3 \pm 2.1	63.2 \pm 3.0
H ₂ GCN	80.6 \pm 0.6	68.2 \pm 0.7	78.5 \pm 0.3	25.6 \pm 1.0	47.3 \pm 0.8	31.3 \pm 0.7	59.8 \pm 3.7	66.3 \pm 4.6	61.5 \pm 4.4
Ortho-GCN	80.6 \pm 0.4	69.5 \pm 0.3	76.9 \pm 0.3	21.4 \pm 1.6	46.7 \pm 0.5	31.3 \pm 0.6	45.4 \pm 4.7	53.1 \pm 3.9	46.6 \pm 5.8
P-reg	80.0 \pm 0.8	69.2 \pm 0.7	77.4 \pm 0.4	20.9 \pm 0.5	49.1 \pm 0.1	33.6* \pm 0.4	44.9 \pm 3.1	58.5 \pm 4.2	53.7 \pm 2.6
ACM-GCN	80.2 \pm 0.8	68.3 \pm 1.1	78.1 \pm 0.5	24.9 \pm 2.0	49.5 \pm 0.7	31.6 \pm 0.4	55.6 \pm 3.3	58.9 \pm 2.6	61.3 \pm 0.5
HOG-GCN	79.7 \pm 0.4	68.2 \pm 0.6	78.0 \pm 0.2	21.5 \pm 0.5	47.7 \pm 0.5	30.1 \pm 0.4	61.8 \pm 0.8	60.4 \pm 0.6	62.7 \pm 0.3
JacobiConv	81.9 \pm 0.6	69.6 \pm 0.8	78.5 \pm 0.4	25.7 \pm 1.2	52.8* \pm 0.9	32.0 \pm 0.6	55.3 \pm 3.4	57.7 \pm 3.6	53.4 \pm 1.6
GloGNN	82.4 \pm 0.3	70.3 \pm 0.5	79.3 \pm 0.2	26.6 \pm 0.7	48.2 \pm 0.3	28.8 \pm 0.8	56.8 \pm 1.1	63.0 \pm 2.9	59.5 \pm 1.3
PTDNet	81.2 \pm 0.9	69.5 \pm 1.2	78.8 \pm 0.5	21.5 \pm 0.6	50.6 \pm 0.9	32.1 \pm 0.7	63.3 \pm 1.1	59.8 \pm 9.2	53.1 \pm 5.6
PTDNet ‡	81.9 \pm 0.6	71.1 \pm 0.8	79.0 \pm 0.2	22.7 \pm 0.6	50.9 \pm 0.3	32.3 \pm 0.5	64.4 \pm 3.3	62.4 \pm 6.0	55.7 \pm 3.7
GPR-GNN	82.2 \pm 0.4	70.4 \pm 0.8	79.1 \pm 0.1	25.4 \pm 0.5	49.1 \pm 0.7	30.5 \pm 0.6	57.1 \pm 1.6	61.2 \pm 0.9	62.4 \pm 1.2
GPRGNN ‡	84.5* \pm 0.2	73.2 \pm 0.5	80.0* \pm 0.2	27.7 \pm 1.3	50.7 \pm 0.4	31.6 \pm 0.4	61.1 \pm 2.8	63.0 \pm 1.4	63.2 \pm 1.5
FAGCN	80.9 \pm 0.5	69.8 \pm 0.6	79.0 \pm 0.5	25.2 \pm 0.8	46.5 \pm 1.1	30.4 \pm 0.4	55.6 \pm 3.0	50.1 \pm 3.9	57.8 \pm 6.5
FAGCN ‡	83.7 \pm 0.4	73.7* \pm 0.5	79.7 \pm 0.2	27.3 \pm 0.5	48.6 \pm 0.7	31.3 \pm 0.5	60.5 \pm 2.9	55.4 \pm 2.6	59.6 \pm 4.6
GGCN	80.0 \pm 1.2	69.7 \pm 1.6	78.2 \pm 0.4	22.5 \pm 0.5	48.5 \pm 0.7	30.2 \pm 0.6	62.8 \pm 4.0	66.4 \pm 1.7	61.7 \pm 3.2
GGCN ‡	83.4 \pm 0.8	73.1 \pm 0.4	78.7 \pm 0.3	24.1 \pm 0.4	49.8 \pm 0.4	30.8 \pm 0.6	66.7* \pm 2.2	69.9* \pm 0.6	62.6 \pm 1.5

F.2. Node classification accuracy of other state-of-the-art methods

In Table 4, we measure the node classification accuracy by adding three datasets and various state-of-the-art baselines. The WebKB graphs *Cornell*, *Texas*, *Wisconsin*⁷ are comprised of the web pages of computer science departments in various universities. Firstly, we briefly introduce the details of newly added methods and their implementation as follows:

- **P-reg** [Yang *et al.*, 2021] ensembles a regularization term to provide additional information that training nodes might not capture. (*source code*⁸)
- **ACM-GCN** [Luan *et al.*, 2022] suggests a local diversification operation through the adaptive channel mixing algorithm. (*source code*⁹)
- **HOG-GCN** [Wang *et al.*, 2022] adaptively controls the propagation mechanism by measuring the homophily degrees between two nodes. (*source code*¹⁰)
- **JacobiConv** [Wang and Zhang, 2022] studies the expressive power of spectral GNN and establishes a connection with the graph isomorphism testing. (*source code*¹¹)
- **GloGNN** [Li *et al.*, 2022] receives information from global nodes, which can accelerate neighborhood aggregation. (*source code*¹²)

In the above table, we can see that signed GNNs with calibration generally outperform the baseline methods. As mentioned before, signed methods achieve inferior performance under the Chameleon and Squirrel datasets, where many nodes share the same neighboring nodes. Instead, in another graph, calibrated GNNs still achieve competitive results. Especially, for WebKB datasets, the average improvement of signed GNNs (GPRGNN, FAGCN, and GGCN) through calibration is 3.7%, 7.5%, and 4.4%, respectively. Throughout this result,

⁷<http://www.cs.cmu.edu/webkb/>

⁸<https://github.com/yang-han/P-reg>

⁹<https://github.com/SitaoLuan/ACM-GNN>

¹⁰<https://github.com/hedongxiao-tju/HOG-GCN>

¹¹<https://github.com/GraphPKU/JacobiConv>

¹²<https://github.com/RecklessRonan/GloGNN>